AIP Journal of Applied Physics

Metastable phase formation in the Au-Si system via ultrafast nanocalorimetry

M. Zhang, J. G. Wen, M. Y. Efremov, E. A. Olson, Z. S. Zhang et al.

Citation: J. Appl. Phys. **111**, 093516 (2012); doi: 10.1063/1.4712342
View online: http://dx.doi.org/10.1063/1.4712342
View Table of Contents: http://jap.aip.org/resource/1/JAPIAU/v111/i9
Published by the American Institute of Physics.

Related Articles

Reduced longitudinal optical phonon-exciton interaction in InGaN/GaN nanorod structures
Appl. Phys. Lett. 100, 182105 (2012)

Preparation of PVA/Co/Ag film and evaluation of its magnetic and microstructural properties
J. Appl. Phys. 111, 094302 (2012)

High-aspect-ratio grooves fabricated in silicon by a single pass of femtosecond laser pulses
J. Appl. Phys. 111, 093102 (2012)

Small copper clusters studied by x-ray absorption near-edge structure
J. Appl. Phys. 111, 084315 (2012)

Photovoltaic effect of individual polymer nanotube
Appl. Phys. Lett. 100, 173902 (2012)

Additional information on J. Appl. Phys.

Journal Homepage: http://jap.aip.org/
Journal Information: http://jap.aip.org/about/about_the_journal
Top downloads: http://jap.aip.org/features/most_downloaded
Information for Authors: http://jap.aip.org/authors

ADVERTISEMENT

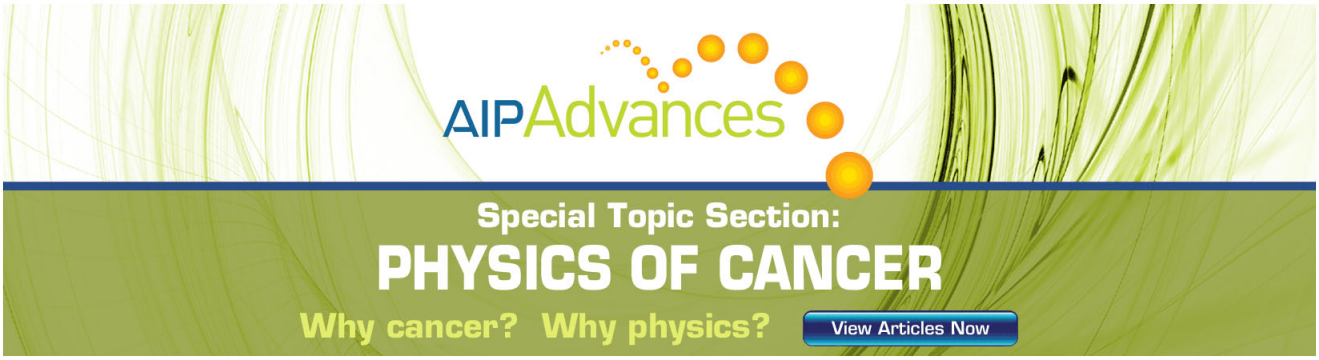

Metastable phase formation in the Au-Si system via ultrafast nanocalorimetry

M. Zhang,[1,a)] J. G. Wen,[2] M. Y. Efremov,[1,b)] E. A. Olson,[1,2] Z. S. Zhang,[1,a)] L. Hu,[1] L. P. de la Rama,[1] R. Kummamuru,[1] K. L. Kavanagh,[3] Z. Ma,[4] and L. H. Allen[1]

[1]*Department of Materials Science and Engineering and Coordinated Science Laboratory, University of Illinois at Urbana-Champaign, Urbana, Illinois 61801, USA*
[2]*Frederick-Seitz Materials Research Laboratory, University of Illinois at Urbana-Champaign, Urbana, Illinois 61801, USA*
[3]*Department of Physics, Simon Fraser University, Burnaby BC V5A 1S6, Canada*
[4]*Intel Corporation, Hillsboro, Oregon 97006, USA*

(Received 23 November 2011; accepted 10 April 2012; published online 7 May 2012)

We have investigated the stability and solidification of nanometer size Au-Si droplets using an ultrafast heating/cooling nanocalorimetry and *in situ* growth techniques. The liquid can be supercooled to very low temperatures for both Au-rich ($\Delta T \sim 95$ K) and Si-rich ($\Delta T \sim 220$ K) samples. Solidification of a unique metastable phase δ_1 is observed with a composition of 74 ± 4 at. % Au and a *b*-centered orthorhombic structure ($a = 0.92$, $b = 0.72$, and $c = 1.35$ nm; body-center in the *a*-*c* plane), which grows heteroepitaxially to Au_s. Its melting temperature T_m is 305 ± 5 °C. There is competition during formation between the eutectic and δ_1 phases but δ_1 is the only metastable alloy observed. For small size droplets, both the δ_1 and eutectic phases show considerable depression of the melting point (size-dependent melting). © *2012 American Institute of Physics*. [http://dx.doi.org/10.1063/1.4712342]

I. INTRODUCTION

Au was the first metallization used for Si or Ge based microelectronics. Au/Ge contacts formed the first transistor[1,2] and the first solid state particle detector.[3] Reactions of Au/Si are the earliest silicide contacts explored.[4] Today, this system is particularly relevant since Si and Ge nanowires,[5] which are used for advanced devices,[3,6,7] are currently grown using nanometer-size liquid $(Au\text{-}Si)_L$ eutectic droplets.[8]

The Au-Si system easily forms metastable crystalline and glassy phases. It also has one of the deepest relative eutectic points ($T_e = 638$ K) and a relatively low glass transition temperature ($T_g \sim 273$ K).[9] Supercooled liquid $(Au\text{-}Si)_L$ obtained via rapid quenching ushered in the first studies of metallic glass.[10–13] All Au-Si crystalline alloys[14] are metastable but can be easily made. The unusual aspects of Au-Si stem from the nature of the supercooled $(Au\text{-}Si)_L$ liquid. It is an extremely fragile liquid[15] and thus unusually stable due to strong local short-range ordering in the liquid. Recent studies[16–19] show that there is additional enhanced ordering at the liquid/solid interface and surface.

There are four levels of ordering in the $(Au\text{-}Si)_L$ liquid: (1) intrinsic ordering[20] as indicated by the large anomalous ($\Delta Cp > 60\%$) specific heat as compared to the vibrational Cp,[21] (2) 2-D solid layer (surface freezing),[16] (3) vertical layering (sheets) of atoms extending up to10 layers (2.5 nm) into the liquid from the top surface,[16] and (4) vertical layering extending from the bottom solid/liquid $Au_s/(Au\text{-}Si)_L$) interface as in the Al/Al_2O_3 case.[18,19] When combining the thicknesses of the 2-D layer, top-surface and bottom-interface layered liquid, the integrated thickness of the ordered liquid is in the order of 5–10 nm, a thickness which is accessible for heat capacity measurements using the ultrasensitive nanocalorimeter device.

Size-dependent melting in the Au-Si system is also of interest and is significant at the 0–10 nm size-scale. It has been previously observed in pure elements,[22–25] compound materials,[26] and eutectic alloys.[27,28] The size of the Au-Si droplets is important for determining practical growth temperatures of nanowires. Size-dependent properties have been studied in our previous nanocalorimetry work on magic-size clusters,[29] glassy polymers,[30] and single layers of alkanethiolate.[31]

In this paper, we explore the supercooling and solidification properties of $(Au\text{-}Si)_L$ liquid using nanocalorimetry, which is sensitive enough to sample the liquid and solids throughout the thickness range of 0–10 nm. At this thickness, size-effect melting is clearly observed in the solidification products. Moreover, the enhanced layer-ordering (sheets) extends throughout all of the liquid being sampled. A schematic diagram is shown in Fig. 1. We find that there is a large increase in the stability of the liquid and the formation of a unique alloy δ_1, which has a well-defined melting peak. We identify the formation path of δ_1, establish the composition boundaries using *in situ* $C_p(T)$ during deposition and then discuss the results in terms of ordered liquid and the interface energy. Our work shows in addition to structure, the stoichiometric, melting, solidification, and stability characteristics of the liquid phase.

II. EXPERIMENT

The operation,[32,33] fabrication,[34] and calibration[33,35] of the nanocalorimeter have been discussed in detail in previous work. In brief, nanocalorimetry is an ultrasensitive thin-film differential scanning calorimetry technique consists of a thin

[a)]Present address: Micron Technology, Inc., Boise, Idaho 83707, USA.
[b)]Present address: University of Wisconsin at Madison, Madison, Wisconsin 53706, USA.

 © 2012 American Institute of Physics

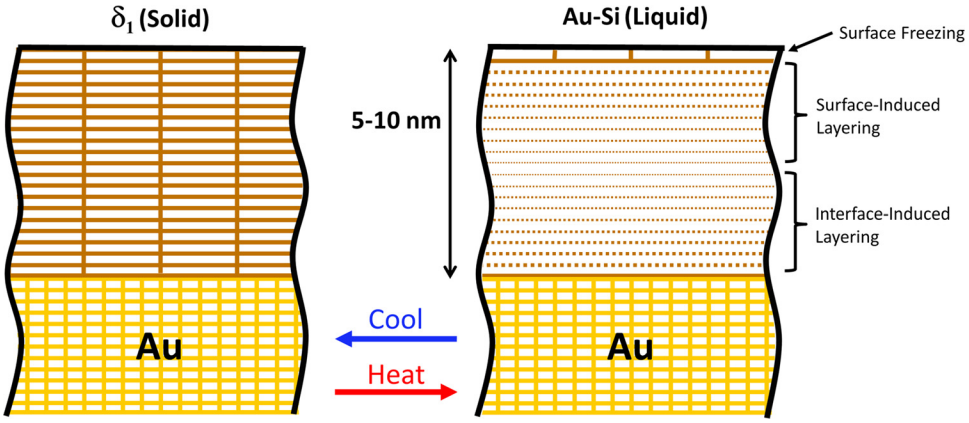

FIG. 1. Schematic diagram of solid δ_1 and liquid Au-Si alloy on gold substrates. Liquid Au-Si shows the 2D surface freezing with the same lattice parameters as δ_1 and the ordering within the liquid due to both the crystalline surface and the $Au_s/(Au\text{-}Si)_L$ interface.

50 nm Si-N membrane supported by a Si frame. Samples are deposited on one side of the membrane and a thin (50 nm) metal heater strip is deposited on the other side. By inducing a short pulse of current through it, the heater serves both to heat the membrane/sample and to measure its temperature. The values of voltage and current across the heater are used for power and temperature calculations, and finally, for the calculation of $C_p(T)$. Very fast heating rate varied from 20 000 to 200 000 K/s allows the nanocalorimeter to operate in nearly adiabatic conditions.

Deposition and Cp measurements are done using a dedicated UHV system with a base pressure of 2×10^{-10} Torr and a Si deposition pressure of $<2 \times 10^{-9}$ Torr in order to abate oxidation effects due to the aggressive nature of metal induced oxidation process.[36,37] The Au-Si δ_1 (Ref. 38) alloy is formed in this study by rapidly cooling (10^4 °C/s) Au-rich, Au-Si samples deposited onto an electron-transparent nanocalorimeter device shown in Fig. 2(a). Using the high heating rate of nanocalorimetry, we reach 450 °C in 10 ms. The average passive cooling rate of 10^4 °C/s is slower than 10^5 °C/s which can induce glass formation[39] but fast enough to form δ_1. The resulting crystals of δ_1 do not change during the short-time for air-transfer required for *ex situ* transmission electron microscopy (TEM) analysis. The stability of δ_1 to ambient air exposure is tested in an experiment where a sample that has already undergone calorimetry measurement is then transferred to another vacuum chamber with an ambient air exposure of 15 min. The second calorimetry measurement shows that the melting peak height of δ_1 was within 10% of the first calorimetry result. This result is in stark contrast to samples exposed to ambient for 2 months or more. In this case, there is no melting peak observed which is expected since all of the Si will be removed from the alloy due to metal induced oxidation.

III. RESULTS AND DISCUSSION

Using electron diffraction (ED), a δ_1 single crystal was analyzed in multiple directions and tilted from [001] to [011] and from [001] to [101] diffraction zone axes. Selected diffraction patterns are presented in Fig. 3(a). Simulation of the ED patterns shows that δ_1 is b-centered orthorhombic ($a = 0.92$, $b = 0.72$, and $c = 1.35 = 2 \times 0.675$ nm) with the body-center in the a-c plane. The ED patterns have regular spots at $h + l = 2n$ and extinctions at $h + l = 2n + 1$, where n is an integer. Notice the different extinctions between the first and the second Laue zones, showing a b-center in the a-c plane. These values are close to those reported for the orthorhombic and surface structures in other studies[16,40–42] after correction for thermal expansion (see Table I). The data reported by Shpyrko[16] for 2D surface freezing on liquid Au-Si alloy were obtained at 360 °C; thus, adjustment for

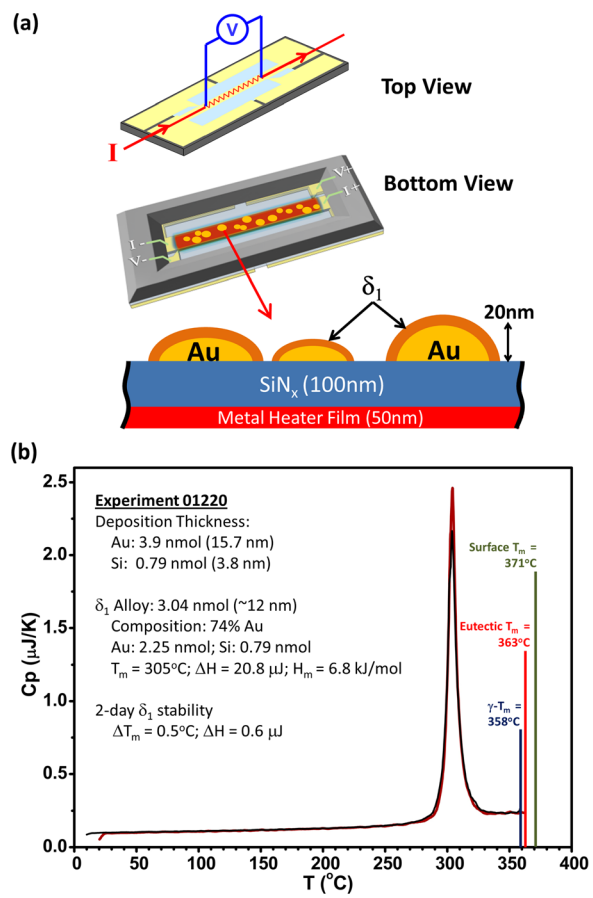

FIG. 2. (a) Schematic of the nanocalorimetry device showing the sample placement. (b) Caloric curves shown with the δ_1 melting peak at 305 ± 5 °C. Two caloric curves from day 0 (black) and day 2 (red) are overlapped and are almost identical. The melting temperature is within 0.5 °C while the heat of fusion is within 3% for the day 0 and day 2 results indicating stability of δ_1 under vacuum. The caloric curves are averages of 50 pulses for each experiment. The baseline of this data set is taken after Si deposition before Au is deposited.

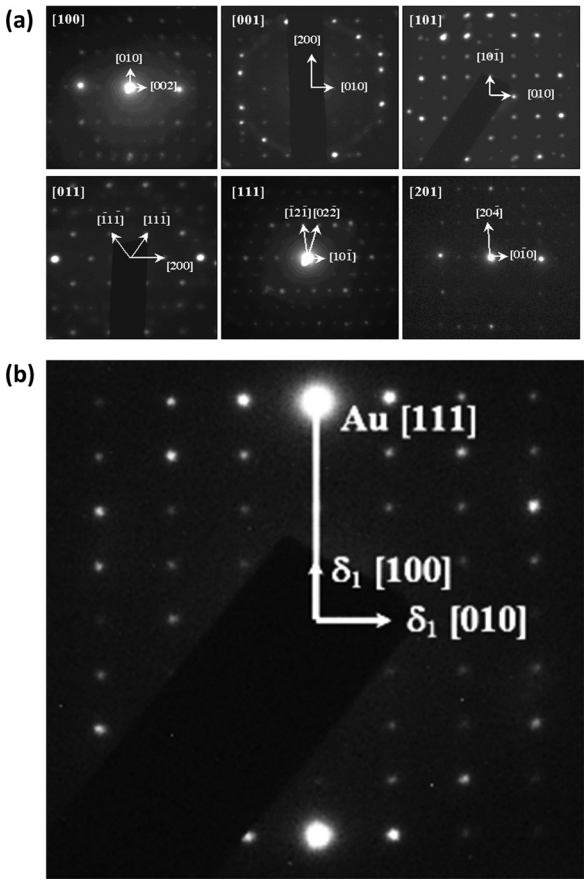

FIG. 3. (a) Diffraction patterns of single crystal δ_1 oriented with the electron beam parallel to [100], [001], [101], [011], [111], and [201] directions. (b) An example of a diffraction pattern for the Au core and δ_1 shell structure (diagrammed) with a δ_1 [001] orientation showing the epitaxial relation between the δ_1 shell on a Au core that is most often observed: Au[111]//4 × δ_1[100].

thermal expansion is necessary to obtain values at room temperature using a thermal expansion coefficient of 15 ppm/°C which is typical for silicides.

δ_1 forms as a crystalline shell around the Au_s core. The ED pattern (Fig. 3(b)) shows that δ_1 has a shared (epitaxial) orientation with Au_s: Au [111]//4 × δ_1 [100]. This result is consistent with a previous study of bi-layers of polycrystalline Au and amorphous-Si,[43] although the crystal structure was not clear from that work. The uniform morphology of the core-shell structure suggests that the liquid easily wets the surface of the Au grain prior to solidification. The heat of melting of this microstructure does not depend on the amount of excess Au, suggesting very low solubility of Si in Au (≪1 at. %).[44]

The melting of δ_1 in a Au-rich sample with Au_s present is shown in the caloric curve in Fig. 2(b). Only a single melting peak (305 ± 5 °C) is observed and it is well below the eutectic point (363 °C). Since there is only one peak, we deduce that all of the liquid solidifies into δ_1. The melting enthalpy H_m (6.8 ± 1.1 kJ/mol-atom) is similar to the reported γ-Au-Si (6.6 kJ/mol-atom).[20] The measured entropy S_m (11.8 ± 1.9 J/mol-atom-K) is reasonable compared to other metal-rich silicides (e.g., 10.5 J/mol-atom-K for Ni_2Si), parent Au_s phase (9.5 J/mol-atom-K), and other FCC metals (8–12 J/mol-atom-K).[45] The results are summarized in Table II. The reported uncertainty in the temperature is a measure of the full width at half maximum of the melting peak of δ_1. This uncertainty is larger than the instrumental error of ±2 °C determined from the calibration of the nanocalorimetry device against a standard class A 100 Ω Pt resistance temperature detector and multiple experiments using the melting point of bulk indium as the standard temperature. The uncertainty in the heat of fusion is calculated from the errors in the determination of the enthalpy of melting and the number of moles. The enthalpy of melting is obtained from the integrated area under the melting peak using Origin™ peak analysis function. The error in the peak area measurement is 1.5% (20.8 ± 0.3 μJ) when comparing different scans taken over 2 days shown in Fig. 2(b). The number of moles of silicon is calculated from the shift in the heat capacity due to silicon divided by its specific heat. The estimated error is 3.6% (0.79 ± 0.03 nmol). In the formation of δ_1 starting with excess gold, the deposited silicon will be fully consumed. The atomic percentage of silicon in δ_1 is obtained from the energy dispersive spectroscopy (EDS) result and the average of the range of composition for the initial formation of δ_1 as discussed below. The error is 15% (0.26 ± 0.04). The calculated error in the molar heat of fusion is 16% (6.8 ± 1.1 kJ/mol) with details of the calculation given below.

$$H_m = \frac{\Delta H}{\text{moles Au} + \text{moles Si}} = \frac{\Delta H}{\text{moles Si}} \times (1 - \text{F}),$$

where F is the atomic % of Au obtained from EDS and the range of composition for the initial formation of δ_1. Thus, $H_m = 20.8 \pm 0.3\ \mu\text{J} \times (1 - 0.74) \pm 0.04/0.79 \pm 0.03$

TABLE I. Comparison of lattice constants.

	a (Å)	b (Å)	c (Å)	Volume (Å^3)	Δ Volume (%)
Baumann[a]	9.71	7.68	7.03	524	17
Gaigher[b]	9.56	7.5	6.8	488	9
This work	9.2	7.2	6.75	447	0
Green[c]	9.35	7.35			
Shpyrko[d]	9.34	7.35			
Shpyrko[d]	(9.39)[e]	(7.39)[e]			

[a]Reference 40.
[b]Reference 41.
[c]Reference 42.
[d]Reference 16.
[e]Reported values at 360 °C.

TABLE II. Thermodynamic properties.

Phase	Tm (°C)	H_m (kJ/mol-atom)	S_m (J/mol-atom-K)	[Au] (at. %)
Metastable[a]	358	6.6 ± 0.6	10.5	81.4
Metastable[b]	305 ± 5	6.8 ± 1.1	11.8 ± 1.9	74 ± 4
Eutectic[c]	363	9.4 ± 0.3	14.8	80.5
Eutectic[a]	363	9.8 ± 0.4	15.4	81.4
Eutectic[b]	360 ± 5	9.0 ± 1.4	14.1 ± 2.2	n/a

[a]Reference 20.
[b]This work.
[c]Reference 52.

nmol = 6.8 ± 1.1 kJ/mol. The largest contribution to the error in H_m is the error in (1 − F) which is 15%.

δ_1 melts (305 °C) at a much lower temperature than the γ-Au-Si phase (358 °C). This is a rare case of the direct thermal analysis of a metastable alloy and to our knowledge the first direct measurement of alloy melting in the Au-Si system. Typically, Au-Si alloys decompose via solid-state processes into the eutectic components. As the temperature increases during the heating cycle, the liquid is a metastable supercooled liquid after δ_1 has melted. Only after the temperature (during the heating-cycle) exceeds the melting point of the eutectic, the liquid is considered to be thermodynamically stable. Thus, both the liquid and the δ_1 are kinetically trapped in the metastable states using this fast-scanning sequence. The cooling curve for this Au-rich (Au_s and δ_1) sample is also shown in Fig. 4.

The composition of δ_1, which will be discussed later, obtained by EDS and the average of the range of composition which shows the initial formation δ_1 when starting with either a Si-rich or a Au-rich sample is 74 ± 4 at. % Au, slightly less than the equilibrium, bulk eutectic point composition (81.4 at. % Au). For this analysis, the SiN_x support film was carefully removed by brief ion-milling so that partially supported large δ_1 single crystals were studied. The magnitude of the error (±4 at. %) is comparable to the difference between Au-Si phases, e.g., Au_3Si has 75 at. % Au and Au_4Si has 80 at. % Au. δ_1 may not be a line-compound since there is appreciable range in the reported lattice constants (see Table I) (a:5%, b:7%, c:4%) and their volume (ΔV:17%).[40,41]

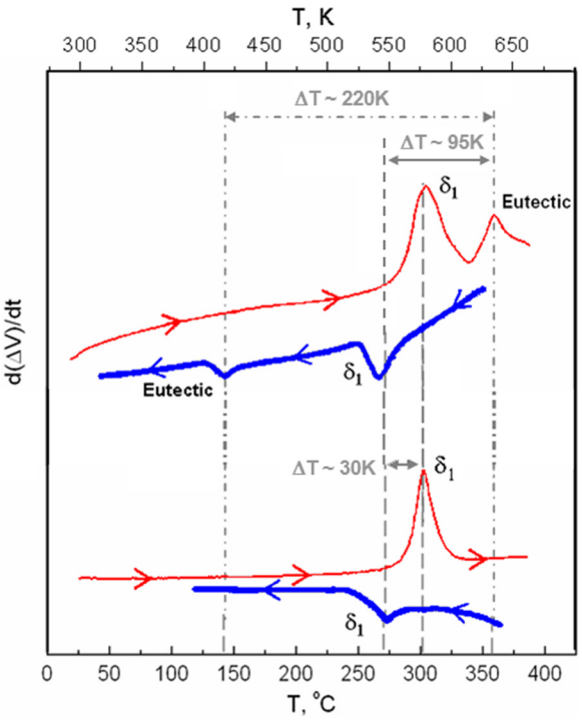

FIG. 4. The heat flow during heating (red) and cooling (blue) from measurement plotted as the time-derivative of the differential voltage, $d(\Delta V)/dt$, versus temperature of Au-Si alloys. (Bottom) Au-rich, single-phase sample: Only one set of melting and solidification peaks are observed corresponding to δ_1; (top) Si-rich, two-phase sample: Au-Si eutectic phase melting and solidification peaks can be found in addition to that from δ_1. The supercooling of δ_1 is ~30 °C, whereas the supercooling of Au-Si eutectic is much larger ~220 °C. The cooling rate is variable but on the order of 10^4 °C/s in both cases.

Given that the presence of Au is important to the formation of δ_1, we explore the melting/solidification using heating/cooling data (Fig. 4) and the boundaries of δ_1 formation over the entire composition range (Fig. 5). By performing nanocalorimetry during deposition,[46] the evolution of the phases is tracked over a large range of average composition. Two separate experiments are done, the first starting with Si-rich conditions and then the reverse experiment with Au-rich conditions.

Results for the first experiment are shown in Fig. 5(a), where 3.7 nm of Si is initially deposited. Au is then slowly evaporated while simultaneously obtaining heating curves. The sample is heated to 450 °C and then cooled after each deposition step. In this way, the average composition is continuously changed with sub-monolayer increments from Si-rich to Au-rich. Only eutectic melting is observed during the early stages of Au deposition when the average composition is Si-rich and ranges from of 0 to 55 at. % Au (0 to 4 nm).

Size-dependent melting of the eutectic is clearly present. The melting point of the eutectic (T_e) gradually increases from 260 °C to the bulk eutectic temperature 363 °C as the amount and size of Au_s crystals increase. TEM results

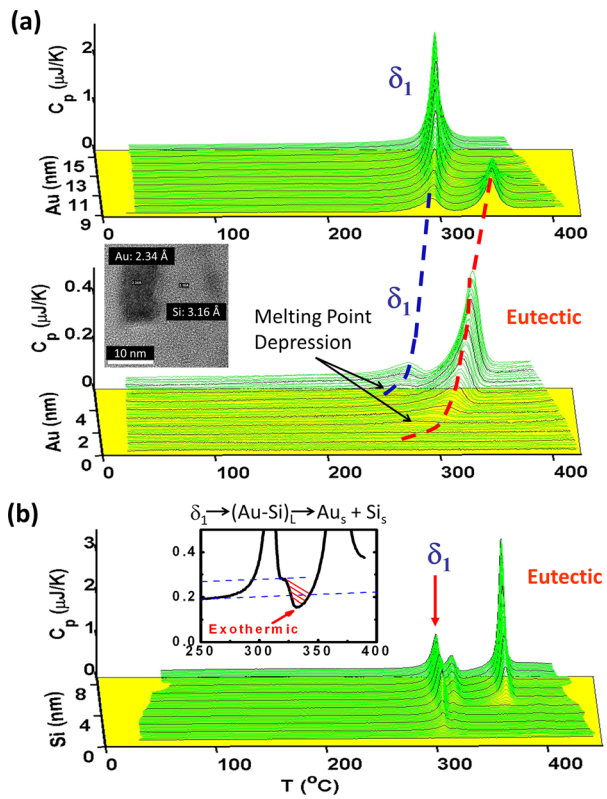

FIG. 5. Three dimensional (3D) $C_p(T, t)$ caloric maps during (a) Au deposition with the sample initially Si-rich and (b) Si deposition with the sample initially Au-rich. Eutectic forms first in (a) followed by δ_1 (Si-rich to Au-rich), whereas δ_1 forms first in (b) followed by the eutectic (Au-rich to Si-rich). Both δ_1 and eutectic are present in Si-rich samples beyond the thickness range shown in (b). Inset in (a) shows TEM lattice images of a 5 nm Au_s (2.34 Å) nanoparticle embedded in a Si_s (3.16 Å) matrix at the early stages of eutectic melting which exhibits melting point depression. Inset in (b) is a Cp(T) plot showing solidification (exothermic) of liquid after δ_1 melts which occurs in the presence of Au(s) and Si(s).

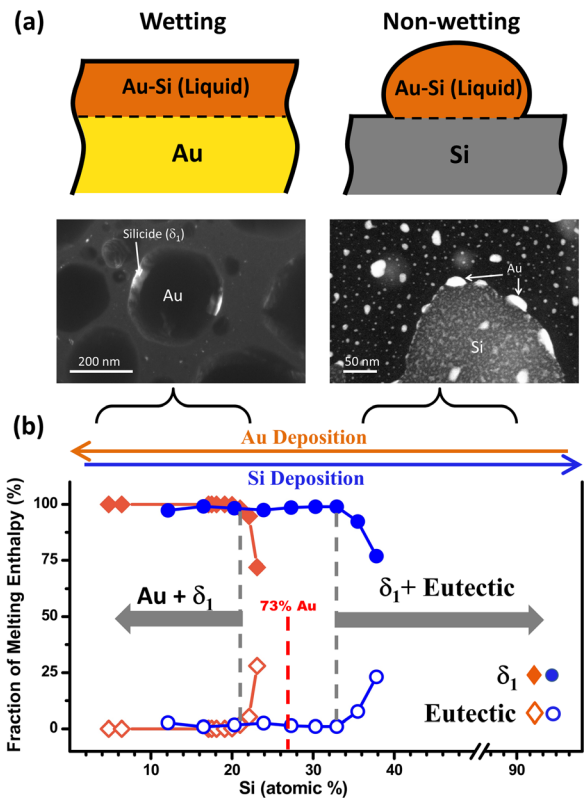

FIG. 6. (a) Schematic of the wettability of δ_1 on Au and Si and TEM micrographs showing high wettability of δ_1 on Au and low wettability of δ_1 on Si. (b) Plot of the fraction of the total melting enthalpy of δ_1 and the eutectic vs. composition for experiments from Fig. 5 with composition changing from 0-95 Si at. % and the reverse 0-95 Au at. %. The median of the range of composition where δ_1 initially forms is 73% ± 6% Au.

confirm that the terminal phases are present with large Si plates in contact with nm-size Au particles (Fig. 6(a)). Each $(Au\text{-}Si)_L$ droplet produces a single crystal Au_s precipitate of roughly 80% the same size. A small Au_s precipitate on a large Si_s plate will have a decrease in melting point. The melting point of the eutectic is 100 K below the bulk T_e which corresponds to nm size Au_s particles using the melting point depression data of Buffat and Borel.[47]

At the composition 55 at. % Au (4 nm), an additional peak due to δ_1 begins to appear at 270 °C. It also exhibits an increase in its melting temperature with increasing thickness and sample volume and in the shape of small 3D particles. With further increases in composition, up to 80 at. % Au (~11.5 nm) and thereafter, only the δ_1 melting peak exists in the caloric curves, consistent with our TEM results. At this final point, the sample is Au-rich with large core-shell particles of Au_s and δ_1 (Fig. 6(a)).

In the second experiment (Fig. 5(b)), the reverse compositional sequence of phase formation is performed by starting with a large amount of Au (12 nm) and then depositing Si and δ_1 is the first and major phase formed. After the average composition becomes Si-rich (<70 at. % Au), the eutectic phase begins to dominate. Unlike the Au deposition case where the eutectic phase disappears when excess Au is supplied, as the Si deposition proceeds, δ_1 continues to persist even with excess Si. A convolution of endothermic (melting of δ_1) and exothermic (re-solidification) processes occurs simultaneously in this temperature region (inset Fig. 5(b)). The $C_p(T)$ below the solid heat capacity line indicates that an exothermic process occurs. This exothermic process is the re-solidification of the liquid (from δ_1) to the eutectic.

Note, in this case we do not observe a significant shift in the melting peak temperature of δ_1. This lack of size effects is due to the impact of geometry and interface energy. In this case, small amounts of $(Au\text{-}Si)_L$ solidify as a thin-shell (platelets)[48,49] of δ_1 covering a very large-radius Au-core. Compare this to that of an ensemble of small spherical particles/droplets of $(Au\text{-}Si)_L$ in contact with Si_s as is the case of the first experiment. Size-effects on spherical particle systems are much larger (3×) than for platelet systems[48,49] for the same size scales when comparing the ratio of surface area to volume. The underlying dissymmetry of the two growth sequence is due to the wetting phenomenon: $(Au\text{-}Si)_L$ wets Au_s but $(Au\text{-}Si)_L$ does not wet Si_s as shown in Fig. 6(a).

We summarize these experiments by evaluating the δ_1 fraction of the total heat of melting as shown in Fig. 6(b). The two curves overlay each other at the critical boundary near 73 at. % Au. We find that δ_1 is the only solidification product in the compositional range of 100-75 at. % Au and corresponds to a two phase ($Au_s + \delta_1$) region. The melting point of δ_1 is invariant (305 °C) over the range of Au-rich composition.

$$Au_s + (Au - Si)_L \underset{Heat}{\overset{Cool}{\rightleftharpoons}} Au_s + \delta_1. \quad (1)$$

The Au-Si system is analogous to the eutectic Pb-Sn system, which also has a metastable (α_1) alloy (50 at. % Sn). In this system, the formation of α_1 is linked to the close lattice constant match between α_1 and the parent Pb(α) phase.[50] Similarly, there is a close lattice match between δ_1 and Au_s.

$$Pb_s + (Pb - Sn)_L \underset{Heat}{\overset{Cool}{\rightleftharpoons}} Pb_s + \alpha_1. \quad (2)$$

We estimate the stoichiometry (73% ± 6% Au) of the δ_1 phase using the data in Fig. 6(b). This provides an additional value for stoichiometry which is independent of EDS analysis. We use the criterion that only δ_1 occurs in Au-rich samples. Then, the stoichiometry of δ_1 should be equal to the average stoichiometry at the minimum Au concentration when only $\delta_1 + Au_s$ are present. We obtain a value of 79% when the deposition sequence is from Si-rich to Au-rich and 67% in the reverse sequence. We speculate that the difference in these values stems from the variation in local stoichiometry of particles due to the distribution of shapes and sizes between the two sequences.

Solidification and the degree of supercooling can be investigated using heating/cooling data in Fig. 4. $(Au\text{-}Si)_L$ liquid is extraordinarily stable when in contact with a Si_s reservoir (seed) without Au_s present. It can be supercooled to T = 513 K (ΔT = 125 K) as shown recently by Schülli *et al.*[17] when cooled at slow rates and to extraordinary low values T = 418 K (ΔT = 220 K) when using faster rates and smaller length scales shown in this work (Fig. 4). $(Au\text{-}Si)_L$ liquid is also extraordinarily stable when in contact with a Au_s reservoir without Si_s present. As shown in Fig. 4, the liquid can be supercooled to T = 578 K (ΔT = 95 K) before solidification.

During the cooling cycle (365–275 °C), the composition of supercooled $(Au\text{-}Si)_L$ liquid remains unchanged when only Si_s (not Au_s) is present. Considering only thermodynamic arguments, all of the Si in $(Au\text{-}Si)_L$ could deposit onto the Si_s, since nucleation is not an impediment for Si growth, and thus reduce the remnant liquid to a Au_L concentrate. However, experimentally the ordered liquid does not allow either Si or Au to be extracted nor nucleation (Au_s) or growth (Si_s) to occur. We conclude that the two possible barriers—growth (small) and nucleation (large)—are not independent but coupled in such a way that both Au_s and Si_s need to be present for eutectic solidification. Similarly, in the case of Au-rich samples (Au_s present and Si_s absent) neither nucleation (Si_s) nor growth (Au_s) occurs. Eutectic solidification occurs at this temperature only when both Au_s and Si_s are present (Fig. 4).

In discussing the details of the initial formation of δ_1 as opposed to that of γ[20], we suggest that this process maybe due to the collective influence of the ordered liquid coupled with the low barrier nucleation sites of the Au_s interface and Au-Si surface layer. The ordered liquid has the same average (and perhaps local) composition as does the δ_1 alloy. Unlike eutectic solidification, formation of δ_1 does not need significant molecular transport or rearrangement on the atomic length scale. In essence, the δ_1 solid is a frozen 3-D version of the ordered liquid. Because of the enhanced ordering by the surface and interface of the confined liquid it is expected to be an even weaker liquid (higher fragility) than the bulk $(Au\text{-}Si)_L$.

Heteroepitaxial nucleation of δ_1 can occur at either (1) the interface of $(Au\text{-}Si)_L$ with the 2D surface lattice ($a = 7.4$, $b = 9.4$) or (2) the interface of $(Au\text{-}Si)_L$ with Au_s. The lattice of the 2D surface and Au_s closely matches two of the lattice parameters of δ_1. Only a small nucleation barrier should exist in both cases since $(Au\text{-}Si)_L$ wets both the Au_s and 2D surface. However, we suggest that the latter (2) process dominates since δ_1 crystal does not easily form without Au_s present and since the orientation of the δ_1 crystal aligns with Au_s lattice. However, the 2D layer maybe inherently aligned with the underlying Au_s surface since they are in close (nm) proximity to each other.

We did not observe the melting ($T_m = 371$ °C) of this surface layer using the nanocalorimetry instrument, perhaps a different experimental design is needed. Assuming that the melting enthalpy scales with that of bulk δ_1, then one layer melting enthalpy would be in the order of $\Delta H = 140$ nJ. This value of heat should be accessible to the nanocalorimeter since we have previously measured single peaks with $\Delta H = 10$ nJ for single crystal polyethylene[51] and $\Delta H = 2.5$ nJ for magic number sized indium clusters.[29]

When considering the governing criteria for the phase-selection of δ_1 over other possible Au-Si alloys (e.g., γ), we do not consider that the cooling rate is a key parameter, since δ_1 forms at a variety of quenching rates ranging from (1 K/s),[41] (10^3 K/s)[40] to (10^4 K/s) the rates used in this work. This is the same range of quench rates used to form other alloys (e.g., γ).[20]

Perhaps a more important selection factor is the small size (nanometer scale) of the liquid and solidification products. Most other Au-Si alloys (e.g., γ (Ref. 20)) form by quenching large bulk liquid samples yielding large particles ~40 000 nm. In contrast, all the previous work[40,41] for δ_1 and work here show small sample sizes in the 15–100 nm range. It is possible that δ_1 is actually the first phase formed for all alloys but it goes undetected because of the miniscule amounts present at the initial stages of solidification—δ_1 may act as the nucleation seed for subsequent formation of other alloys.

IV. CONCLUSION

In summary, we have investigated the stability and solidification of nanometer size Au-Si droplets using an ultrafast heating and cooling nanocalorimetry technique. The liquid can be supercooled and is stable to very low temperatures for both Au-rich and Si-rich samples. Solidification of a unique metastable phase δ_1 is observed. Competition between the eutectic and a metastable phase has been observed but δ_1 is the only metastable alloy observed after rapid cooling of the melt to room temperature at the rate of 10^4 °C/s. TEM data show it to have a b-centered orthorhombic structure with lattice parameters which are closely matched to Au_s. For small size droplets, both the metastable and eutectic phases show considerable depression of the melting point (size-dependent melting).

ACKNOWLEDGMENTS

We gratefully acknowledge P. Infante of CNF at Cornell University for assistance in the fabrication of the nanocalorimeters, and L. Hess and D. Jeffers for encouragement in the use of the new technique and for useful discussions. Special thanks to Jim Mayer for his useful discussions of the unique, mysterious and useful Au-Si system. We also would like to acknowledge L. C. Feldman and K. N. Tu for their fruitful discussions and insights into the study of thin films. This work is supported by the NSF-DMR 9726458, NSF-DMR 1006385 and partial support from INTEL, NSF-0622117, and NSF-0735286. Microanalysis characterization was performed at the Frederick Seitz Materials Research Laboratory Center for Microanalysis of Materials, University of Illinois, which is partially supported by the U.S. Department of Energy under Grant Nos. DE-FG02-07ER46453 and DE-FG02-07ER46471.

[1] J. Bardeen and W. H. Brattain, Phys. Rev. **74**, 230–231 (1948).
[2] W. Shockley, M. Sparks, and G. K. Teal, Phys. Rev. **83**, 151–162 (1951).
[3] J. W. Mayer and B. Gossick, Rev. Sci. Instrum. **27**, 407 (1956).
[4] M.-A. Nicolet and S. S. Lau, in *VLSI Electronics Microstructure Science*, edited by N. G. Einspruch and G. B. Larrabee (1983), Vol. 6, p. 329.
[5] S. Kodambaka, J. Tersoff, M. C. Reuter, and F. M. Ross, Science **316**, 729 (2007).
[6] J. Xianh, W. Lu, Y. Hu, Y. Wu, H. Yan, and C. M. Lieber, Nature **441**, 489 (2006).
[7] K.-C. Lu, W.-W. Wu, H.-W. Wu, C. M. Tanner, J. P. Chang, L. J. Chen, and K. N. Tu, Nano Lett. **7**, 2389 (2007).
[8] R. S. Wagner and W. C. Ellis, Appl. Phys. Lett. **4**, 89 (1964).
[9] R. R. Chromik, L. Zavalij, M. D. Johnson, and E. J. Cotts, J. Appl. Phys. **91**, 8992 (2002).
[10] W. Klement, R. H. Willens, and P. Duwez, Nature **187**, 869 (1960).
[11] T. R. Anantharaman, H. L. Luo, and W. Klement, Nature **210**, 1040 (1966).

[12]P. Duwez, J. Vac. Sci. Technol. B **1**, 218 (1983).
[13]H. S. Chen and D. Turnbull, Appl. Phys. Lett. **10**, 284 (1967).
[14]L. Hultman, A. Robertsson, H. T. G. Hentzell, I. Engstrom, and P. A. Psaras, J. Appl. Phys. **62**, 3647 (1987).
[15]C. A. Angell, K. L. Ngai, G. B. McKenna, P. F. McMillan, and S. W. Martin, J. Appl. Phys. **88**, 3113–3157 (2000).
[16]O. G. Shpyrko, R. Streitel, V. S. K. Balagurusamy, A. Y. Grigoriev, M. Deutsch, B. M. Ocko, M. Meron, B. H. Lin, and P. S. Pershan, Science **313**, 77–80 (2006).
[17]T. U. Schülli, R. Daudin, G. Renaud, A. Vaysset, O. Geaymond, and A. Pasturel, Nature **464**, 1174–1177 (2010).
[18]S. H. Oh, Y. Kauffmann, C. Scheu, W. D. Kaplan, and M. Ruhle, Science **310**, 661 (2005).
[19]A. L. Greer, Nature Mater. **5**, 13–14 (2006).
[20]H. S. Chen and D. Turnbull, J. Appl. Phys. **38**, 3646 (1967).
[21]C. A. Angell, Science **267**, 1924–1935 (1995).
[22]M. Takagi, J. Phys. Soc. Jpn. **9**, 359 (1954).
[23]G. L. Allen, R. A. Bayles, W. W. Gile, and W. A. Jesser, Thin Solid Films **144**, 297–308 (1986).
[24]S. L. Lai, J. Y. Guo, V. Petrova, G. Ramanath, and L. H. Allen, Phys. Rev. Lett. **77**, 99–102 (1996).
[25]D. L. Zhang and B. Cantor, Acta Metall. Mater. **39**, 1595–1602 (1991).
[26]A. N. Goldstein, C. M. Echer, and A. P. Alivisatos, Science **256**, 1425–1427 (1992).
[27]L. S. Palatnik and B. T. Boiko, Phys. Met. Metallogr. **11**, 119 (1961).
[28]W. A. Jesser, R. Z. Shneck, and W. W. Gile, Phys. Rev. B **69**, 144121 (2004).
[29]M. Y. Efremov, F. Schiettekatte, M. Zhang, E. A. Olson, A. T. Kwan, R. S. Berry, and L. H. Allen, Phys. Rev. Lett. **85**, 3560–3563 (2000).
[30]M. Y. Efremov, E. A. Olson, M. Zhang, Z. Zhang, and L. H. Allen, Phys. Rev. Lett. **91**, 85703 (2003).
[31]L. Hu, L. P. de la Rama, M. Y. Efremov, Y. Anahory, F. Schiettekatte, and L. H. Allen, J. Am. Chem. Soc. **133**, 4367–4376 (2011).
[32]S. L. Lai, G. Ramanath, L. H. Allen, P. Infante, and Z. Ma, Appl. Phys. Lett. **67**, 1229–1231 (1995).
[33]M. Y. Efremov, E. A. Olson, M. Zhang, F. Schiettekatte, Z. S. Zhang, and L. H. Allen, Rev. Sci. Instrum. **75**, 179 (2004).
[34]E. A. Olson, M. Y. Efremov, M. Zhang, Z. S. Zhang, and L. H. Allen, J. Microelectromech. Syst. **12**, 355–364 (2003).
[35]M. Y. Efremov, E. A. Olson, M. Zhang, S. L. Lai, F. Schiettekatte, Z. S. Zhang, and L. H. Allen, Thermochim. Acta **412**, 13–23 (2004).
[36]J. M. E. Harper, A. Charai, L. Stolt, F. M. d'Heurle, and P. M. Fryer, Appl. Phys. Lett. **56**, 2519 (1990).
[37]A. Hiraki, E. Lugujjo, and J. W. Mayer, J. Appl. Phys. **43**, 3643–3649 (1972).
[38]G. A. Andersen, J. L. Bestel, A. A. Johnson, and B. Post, Mater. Sci. Eng. **7**, 83 (1971).
[39]J. Schroersa, B. Lohwongwatana, W. L. Johnson, and A. Peker, Appl. Phys. Lett. **87**, 061912 (2005).
[40]F. H. Baumann and W. Schroter, Phys. Rev. B **43**, 6510 (1991).
[41]H. L. Gaigher and N. G. Van der Berg, Thin Solid Films **68**, 373 (1980).
[42]A. K. Green and E. Bauer, J. Appl. Phys. **47**, 1284 (1976).
[43]M. Seibt, S. Buschbaum, U. Gnauert, and W. Schroter, Phys. Rev. Lett. **80**, 774 (1998).
[44]T. B. Okamoto and H. Massalski, *Phase Diagram of Binary Gold Alloys* (ASM International, 1987).
[45]O. Kubaschewski and C. B. Alcook, *Metallurgical Thermochemistry*, 5th ed. (Pergamon, New York, 1979), Vol. 24.
[46]M. Zhang, M. Y. Efremov, E. A. Olson, S. Zhang, and L. H. Allen, Appl. Phys. Lett. **81**, 3801–3803 (2002).
[47]P. Buffat and J. P. Borel, Phys. Rev. A **13**, 2287–2298 (1976).
[48]K. K. Nanda, S. N. Sahu, and S. N. Behera, Phys. Rev. A **66**, 013208 (2002).
[49]Q. Jiang, H. Y. Tong, D. T. Hsu, K. Okuyama, and F. G. Shi, Thin Solid Films **312**, 357 (1998).
[50]H. J. Fecht and J. H. Perepezko, Metall. Trans. A **20A**, 785 (1989).
[51]A. T. Kwan, M. Y. Efremov, E. A. Olson, F. Schiettekatte, M. Zhang, P. H. Geil, and L. H. Allen, J. Polym. Sci., Part B: Polym. Phys. **39**, 1237–1245 (2001).
[52]R. Castanet and C. Bergman, Ann. Chim. Fr. **4**, 419 (1979).